(Received 22 August 2025, Accepted 24 November 2025, Scheduled 22 December 2025)

Experimental Validation of the UHF RFID Dipole Tag Antenna Applied in the Supply Chain

Pape W. Sarr[1, *], Aminata Diop[1], Arnaud Vena[2], and Ibra Dioum[1]

[1] *Laboratoire d'Informatique, de Télécommunictions et Application (LITA), Polytechnic Institute (ESP) Cheikh Anta Diop University (UCAD), Dakar, Senegal*
[2] *Institut d'Electronique et des Systèmes (IES), Montpellier University, Montpellier, France*

ABSTRACT: This paper presents a passive UHF RFID dipole antenna designed for object identification in supply chain applications. The antenna features a simple structure measuring $75 \times 28 \times 1.6\,\text{mm}^3$ ($2.17 \times 0.81 \times 0.046\lambda_0$), with a copper radiating element printed on Taconic RF-35A2 substrate. It is matched to a Monza R6 chip with an impedance of $13 - \text{j}125\,\Omega$ at 868 MHz through a T-matching circuit. The prototype was tested on various complex surfaces, including plastic bottles, foam, cardboard, plastic boxes, and wood. Its performance evaluation involved measuring the reading distances in these environments. Simulation and measurement results demonstrate effective impedance matching between the antenna and chip. The read distances vary with the surface type, with the maximum distance reaching up to 14 meters on a plastic bottle within the European UHF RFID band ((865.5–869.5) MHz) and the shortest distance around 6 meters on wood. Overall, the tag exhibits strong adaptability to different surfaces. Simulations were conducted using CST Studio microwave software.

1. INTRODUCTION

Radio Frequency Identification (RFID) is a technology that employs high-frequency radio waves to transmit and store data for the unique identification of objects, animals, or humans. It finds extensive applications across diverse fields such as supply chain management [1], healthcare [2, 3], animal breeding through implanted tags [4], and the Internet of Things (IoT) [5–7].

Passive RFID systems use tags that communicate with a reader, which powers and interrogates them [8]. This communication relies on the transmission of electromagnetic waves from the reader to the tag [9]. The reader continuously emits a signal, which provides the energy needed to activate the chip embedded in the tag. Once activated, the tag responds by backscattering the signal via its antenna.

RFID systems operate over multiple frequency bands, depending on the application and geographic region. The Ultra-High Frequency (UHF) band (860–960 MHz) is the most widely used due to its long read range compared to the Low Frequency (LF) and High Frequency (HF) bands, with the latter often employed for Near Field Communication (NFC) [9]. The passive UHF RFID technology, requiring no internal battery, allows easy integration and offers significant benefits [10].

Numerous studies have focused on the design of UHF RFID dipole antennas for operation on complex surfaces. For example, a UHF RFID antenna the size of a smart card is proposed in [11] for contactless payment cards such as VISA and MasterCard, achieving a maximum read distance of 12 meters. RFID antennas for identifying liquid-filled bottles are presented in [12, 13], with one design employing a folded dipole and loop matching adapted to the chip, reaching a 5.6-meter read range on water bottles in the American UHF band, though affected by the water surface. The dielectric effects of food and beverage contents and packaging are analyzed in [13]. Another RFID tag dipole, equipped with an integrated Artificial Magnetic Conductor (AMC), with dual bands, namely the European (855–867 MHz) and Japanese (950–955 MHz) UHF RFID bands, was proposed in [14]. This tag, mounted on a metal surface, achieves a read range of 7.3 m at 866 MHz and 10.8 m at 953 m. In [15] and [16, 17], a monopole RFID tag and a dipole RFID tag are proposed. These tags are used to identify objects such as foam, fiber, glass, plastic, and wood. The monopole [15] operates only on the 915 MHz band, while the dipole [16] operates on the 866 MHz and 915 MHz frequency bands.

Efficient transportation of goods requires accurate tracking and traceability from the point of shipment to final delivery, in order to ensure increased product safety and improved operational quality [18]. To meet these requirements, the transportation and logistics sector must undergo a digital transformation by implementing systems for identifying and tracking products from source to destination. RFID technology appears to be a particularly suitable solution in this context, as it allows products to be labeled with RFID tags for seamless tracking and identification [19, 20]. Transportation is a key application area for RFID due to the considerable volume of goods transported from one location to another. These goods are often packaged in cardboard boxes or wooden crates [21]. Unlike barcodes, which require contact identification, RFID enables contactless, intelligent identification by facilitating communication between the reader and the tag through electromagnetic wave backscatter [22–25].

* Corresponding author: Pape Waly Sarr (papewaly.sarr@esp.sn).

This paper presents a meandered dipole RFID tag antenna designed for product tracking in the supply chain. The work carried out in this paper presents a new method for improving the performance of a dipole antenna. This method is based on the use of short-circuit stubs, which not only adjust the impedance matching between the antenna and the chip, but also improve the tag's performance in terms of gain and read range compared to the reference design. This design approach offers a practical and effective solution for applications requiring good performance in compact formats. The addition of stubs extends the tag's inductive lines, enabling precise resonance tuning at 868 MHz and achieving effective impedance matching with the Monza R6 chip. The fabricated prototype demonstrated excellent performance, reaching a maximum reading range of 14 m on a plastic bottle and a minimum read range of 6 m on wood surface. This robust performance is highly beneficial for real-world supply chain application where goods are packaged in diverse materials.

2. PROPOSED RFID TAG DIPOLE

The proposed tag antenna in this paper is a meander-shaped dipole with a simple design, as shown in Figure 1. It consists of a copper dipole etched onto a 1.6 mm thick FR4 epoxy substrate ($\varepsilon_r = 4.4$ and $\tan\sigma = 0.02$). The overall tag dimensions are $75 \times 28 \times 1.6\,\text{mm}^3$ ($2.17 \times 0.81 \times 0.046\lambda_0$). The antenna design was initially simulated in free space using the HFSS (High Frequency Structure Simulator) software.

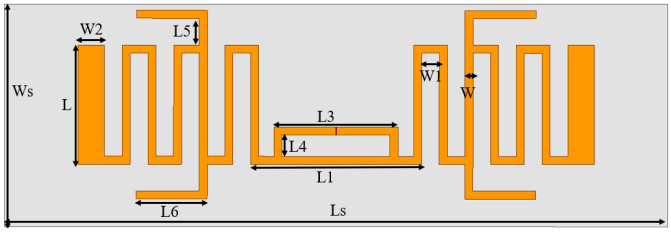

FIGURE 1. Proposed passive UHF RFID tag dipole antenna.

The initial design started with a simple meander dipole serving as a reference antenna, without any short-circuit stubs. This reference antenna is connected to a T-shaped matching network, which is specifically designed to interface with the Monza R6 chip characterized by an impedance of $(13 - j125)\,\Omega$ at 868 MHz. The measured reflection coefficient reveals that the antenna resonates at 903 MHz MHz with an S_{11} of -19.8 dB (Figure 2). However, this resonance frequency falls within the (900–910) MHz band, which lies outside the desired operational frequency range of (865.5–869.5) MHz for the European UHF RFID band. This mismatch in frequency highlights the need for further tuning of the antenna geometry or matching network to align the resonance with the target band.

To analyze areas of high and low current density for optimizing the design parameters, we simulated the surface current distribution. Figure 3 shows that the current is predominantly concentrated around the matching circuit, whereas the meandering lines exhibit low current density. Consequently, increasing the length or width of these lines will have minimal impact on the

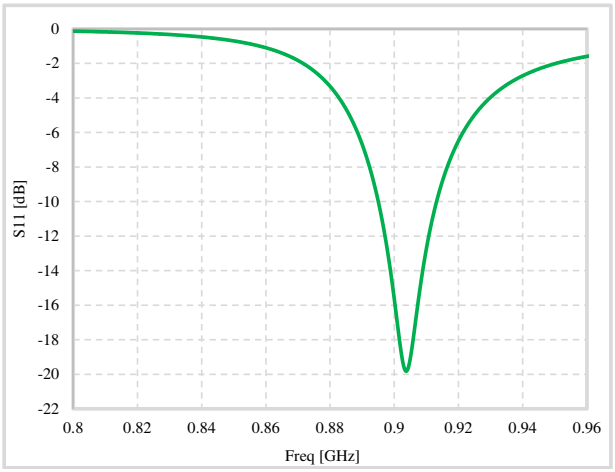

FIGURE 2. Reflection coefficient of the reference antenna.

antenna's resonance frequency. Therefore, an alternative technique is necessary to shift the frequency and achieve resonance at the target frequency of 868 MHz.

To increase areas of high current density, we introduced two short-circuit stubs on the upper sections of the dipole arms. These stubs are placed symmetrically with respect to the matching network (Figure 4). This configuration is intended to concentrate the current in these regions, thereby enabling effective resonance tuning.

The simulated current density for the dipole antenna connected to the two short-circuit stubs remains low, similar to the previous configuration. The current is mainly concentrated near the chip area, while the current intensity along the radiating lines is very weak. As a result, the resonance frequency does not shift, and the antenna still resonates at 903 MHz with a reflection coefficient of -15 dB, as shown in Figure 5.

Another pair of stubs was added symmetrically with respect to the first pair (Figure 6). These additional stubs extend the electrical length of the dipole, thereby enhancing the inductive reactance of the antenna. The simulated current density now shows a more uniform distribution over the entire radiating surface, with a stronger concentration near the matching network. Connecting folded-over lines in regions of high current significantly impacts the resonance frequency, effectively lengthening the meander lines and allowing the antenna to resonate at lower frequencies. Through a parametric study on the line lengths, this method successfully shifted the antenna's resonance to cover the European UHF RFID band, as illustrated in Figure 7.

The use of stubs to short-circuit the dipole's meander lines has not only made it possible to adjust the resonance to cover the European UHF RFID band, but also to increase the tag's gain and radiation efficiency. This improves its radiation performance. The four short-circuit stubs used in this design demonstrate the difference between the proposed dipole and conventionally used dipoles.

Table 1 summarizes the tag parameters along with their corresponding values, which were derived from these parametric analyses to achieve the best impedance matching.

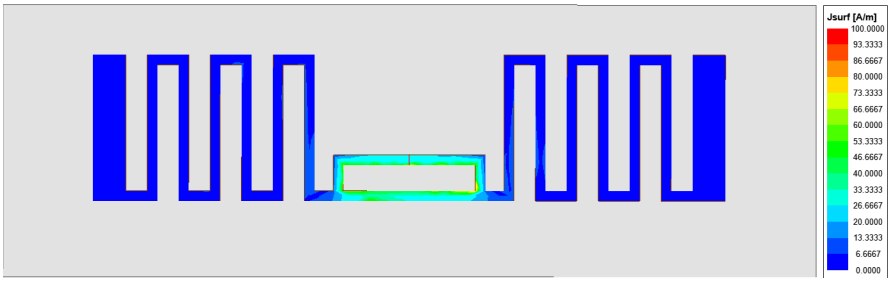

FIGURE 3. Simulated current density without short-circuit.

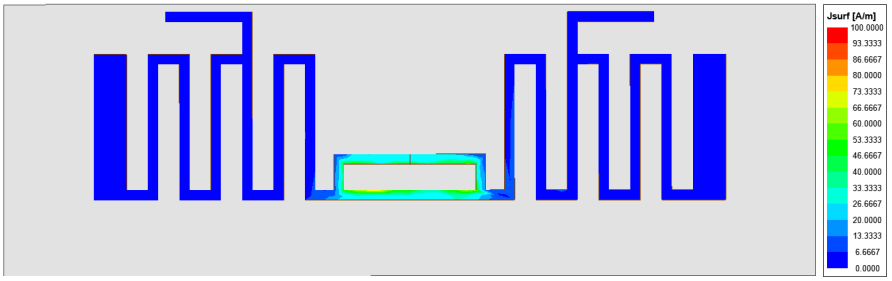

FIGURE 4. Simulated current density with two stubs.

TABLE 1. Antenna parameters and their values (in mm).

Parameters	L_s	W_s	L	L_1	L_2	L_3
Values (mm)	75	25	13.4	17.5	3	14
Parameters	L_4	L_5	L_6	W	W_1	W_c
Values (mm)	2.4	3	8	0.9	2	0.1

The space left to place the chip is 100 µm due to its small size.

The antenna is connected to Impinj's Monza R6 microchip of size 464.1 µm ×442 µm whose datasheet is given in [26]. Chip parameters are reported in Table 1.

Table 2 summarizes the characteristics of the Monza R6 chip.

TABLE 2. Monza R6 microchip characteristics.

C_p	R_p	C_{mount}	Reading sensitivity	Writing sensitivity
1.23 pF	1.2 kΩ	0.21 pF	−20 dBm	−16.7 dBm

C_p and R_p represent the chip's parallel capacitance and resistance, respectively, while C_{mount} denotes the parasitic capacitance caused by adhesive mounting. The total capacitance is thus the sum of these two components: $C_T = C_p + C_{\text{mount}}$. The chip impedance is calculated using the following equation.

$$Z_{\text{chip}} = Z_{\text{eq}} = \frac{Z_1 Z_2}{Z_1 + Z_2} = \frac{(R_1 + jX_1)(R_2 + jX_2)}{(R_1 + R_2)(X_1 + X_2)} \quad (1)$$

With,

$$\begin{aligned} R_1 &= 1200\,\Omega, \\ R_2 &= 0, \\ X_1 &= 0, \\ X_2 &= -j\Big/(2\pi f C_T) \\ &= -j\Big/\left(2\pi \times 868 \cdot 10^6 \times 1.44 \cdot 10^{-12}\right) \\ &= -\text{j}127.33\,\Omega. \end{aligned} \quad (2)$$

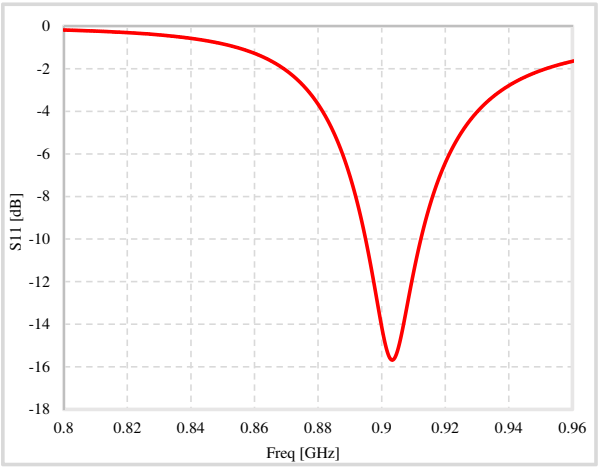

FIGURE 5. Reflection coefficient of the RFID tag antenna with two stubs.

This IC microchip features a low power sensitivity of −22.1 dBm and has an impedance of $Z_{\text{chip}} = 13 - \text{j}125\,\Omega$ at the central European UHF RFID frequency of 868 MHz. Its small size and low sensitivity make it highly efficient and practical. However, the main constraint lies in the chip

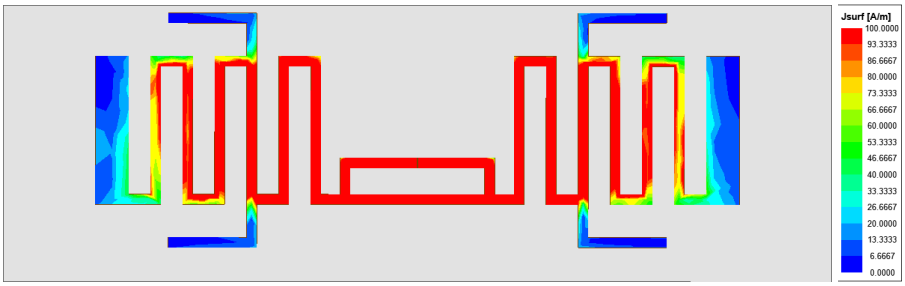

FIGURE 6. Simulated current density of proposed tag dipole antenna.

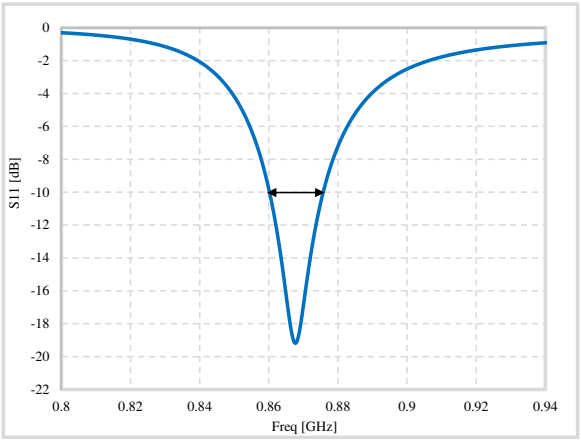

FIGURE 7. Simulated reflection coefficient of the tag antenna.

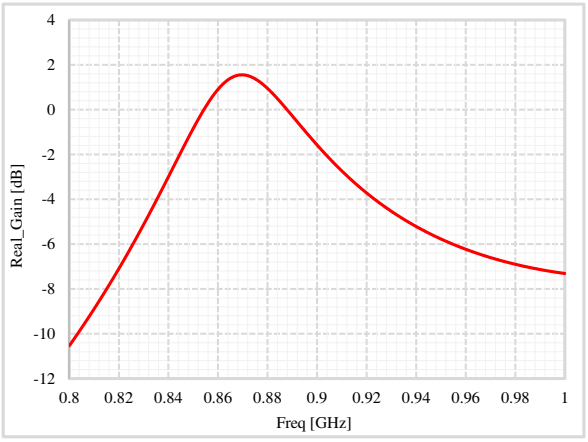

FIGURE 9. Simulated realized gain of the tag antenna.

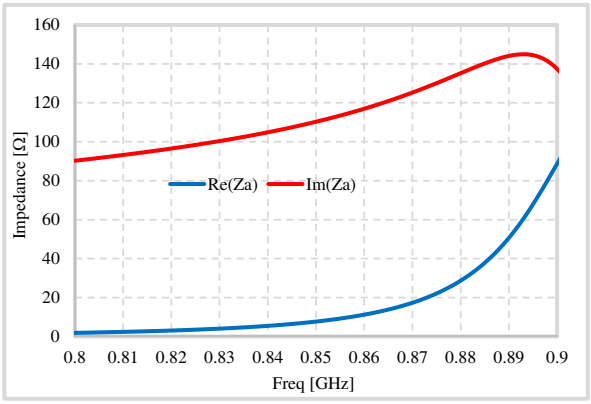

FIGURE 8. Simulated tag antenna impedance.

attachment process, which requires additional tools to ensure secure mounting.

3. SIMULATION RESULTS

The power reflection coefficient (Figure 7) and impedance (Figure 8) were simulated to evaluate the dipole antenna's performance in terms of resonance and impedance matching. The tag antenna resonates at the European UHF RFID center frequency of 868 MHz, covering a bandwidth of 15.7 MHz (860–875.7 MHz) with a matching criterion of -10 dB, which corresponds to a 10% power loss. At the resonant frequency (868 MHz), the simulated return loss is $S_{11} = -19$ dB.

The simulated tag impedance is $Z_a = 15.7 + \mathrm{j}123.5\,\Omega$, which closely matches the conjugate of the chip impedance ($Z_c^* = 13 + \mathrm{j}125\,\Omega$) at 868 MHz (Figure 8). This impedance matching ensures that the antenna can efficiently transfer the maximum amount of energy received from the reader's signal to the chip.

Key radiation parameters of the antenna, including the radiation pattern, gain, and radiation efficiency, were simulated to evaluate its electromagnetic performance comprehensively.

The gain shown in Figure 9 represents the realized gain of the tag over the 0.8 to 1 GHz frequency range. Realized gain is a crucial parameter that directly influences the tag's reading distance by accounting for both antenna gain and impedance matching losses. The simulation results indicate a realized gain of 1.55 dB at 868 MHz, demonstrating the antenna's effective radiation performance within the European UHF RFID band.

Figure 10 illustrates the tag's radiation efficiency across the 0.8 to 1 GHz frequency band. Radiation efficiency is defined as the ratio of the power radiated by the antenna to the total power received at its input. The results indicate that the tag achieves a high radiation efficiency of up to 87% at 868 MHz, which signifies minimal ohmic losses and effective power radiation within the European UHF RFID band. With an efficiency of 87%, there will be good transmission of the energy received by the tag antenna to the Monza R6 microchip.

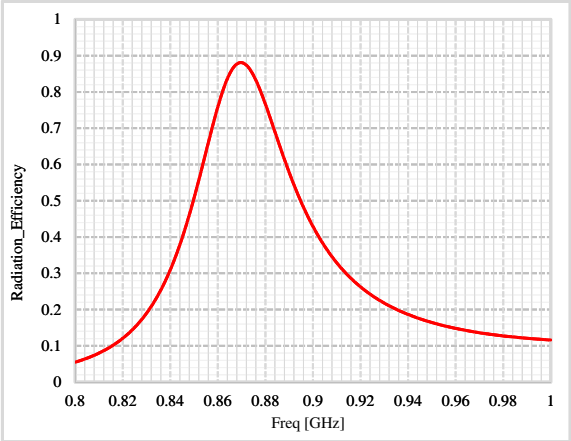

FIGURE 10. Simulated radiation efficiency.

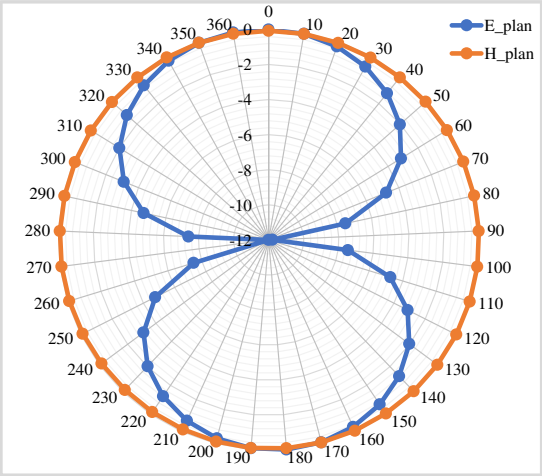

FIGURE 11. Simulated radiation pattern at 868 MHz.

Figure 11 presents the 2D radiation patterns of the tag in both the horizontal (H) and vertical (E) planes at 868 MHz. The antenna exhibits an omnidirectional radiation pattern, characteristic of many dipole-type RFID tag antennas [14–16]. This omnidirectional coverage ensures wide area tracking capability, allowing the tag to reliably identify objects regardless of their orientation relative to the reader.

To evaluate the impact of complex surfaces on the prototype, the tag was mounted on various substrates including a polyethylene terephthalate (PET) plastic bottle, a glass bottle, wood, foam, and cardboard. The electrical and physical properties of these surfaces, which can influence the tag's performance by affecting antenna parameters such as impedance, resonance frequency, and radiation efficiency, are summarized in Table 3 [26–29].

To evaluate its performance, the tag was mounted on various surfaces. Figure 12 presents the simulated reflection coefficient of the tag in free space and on different substrates, including plastic and glass bottles, foam, cardboard, and wood. When placed on foam or a plastic bottle, the tag's performance remains close to that in free space, exhibiting good impedance

TABLE 3. Dielectric properties of the different surfaces.

Surfaces	PET	Glass	Wood	Foam	Cardboard
ε_r	3	5.5	1.7	1.03	1.78
$\tan\sigma$	0.002	0.0	0.036	0.0001	0.025

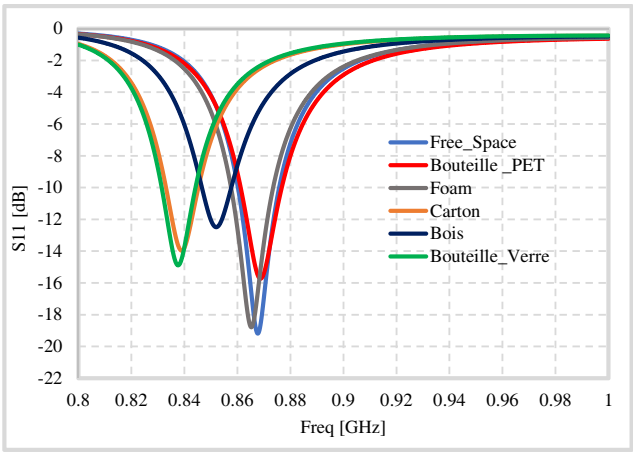

FIGURE 12. Simulation of tag reflection coefficient on different surfaces.

matching. However, mounting the tag on cardboard, wood, or a glass bottle causes a resonance shift towards lower frequencies, leading to increased matching losses within the desired band. This resonance shift also adversely impacts radiation characteristics such as antenna gain and read range.

Figure 13 shows the tag's maximum read distance $d_{\max}$ on the different surfaces to be tagged, determined from the FRISS equation given by Equation (3) [30].

$$d_{\max} = \frac{\lambda}{4\pi}\sqrt{\frac{\text{EIRP}\, G_R \tau}{P_{\text{th}}}} \tag{3}$$

where $\text{EIRP} = P_e G_e$ is the Effective Isotropic Radiated Power, normalized to 3.28 W in the European UHF RFID band; P_e and P_{th} correspond to the reader's transmitting power and the chip's sensitivity, respectively; G_e et G_R are the gains of the reader and tag antennas, respectively. The transmission coefficient τ is calculated from Equation (4) ($\tau = 0.99$).

$$\tau = 1 - |\Gamma|^2 = 1 - S_{11}^2 \tag{4}$$

With,

$$\Gamma = \frac{Z_a - Z_c^*}{Z_a + Z_c} \tag{5}$$

The reading range varies depending on the surface type, as the properties of these materials influence the tag's impedance matching and radiation performance. Although dipole antennas are typically sensitive to complex surfaces, simulation results show that the read range, calculated with an EIRP of 3.28 W [31], exceeds 6 meters for all tested surfaces. This demonstrates that the proposed tag is well suited for its intended application in product identification.

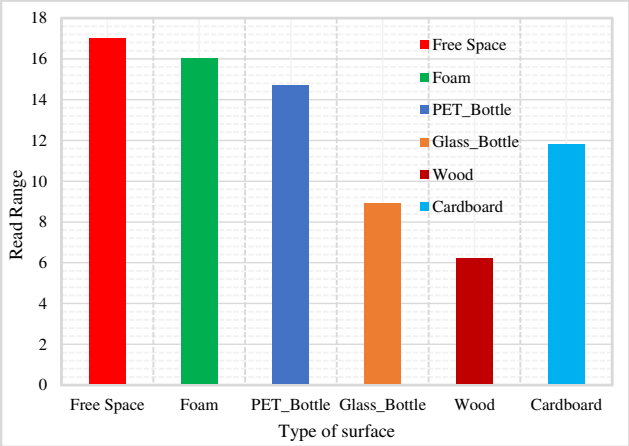

FIGURE 13. Simulated reading distance on various complex surfaces.

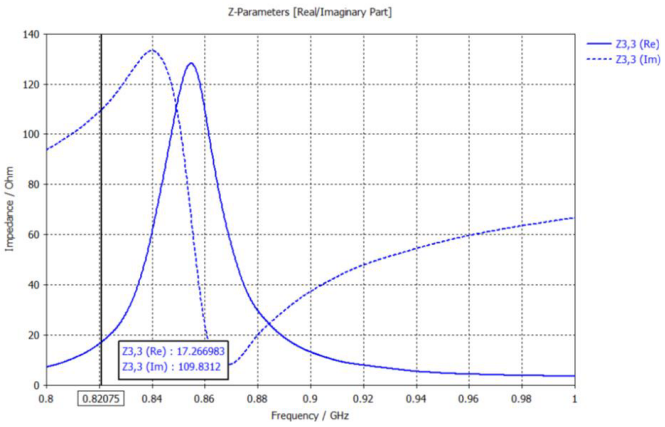

FIGURE 15. Measured tag impedance.

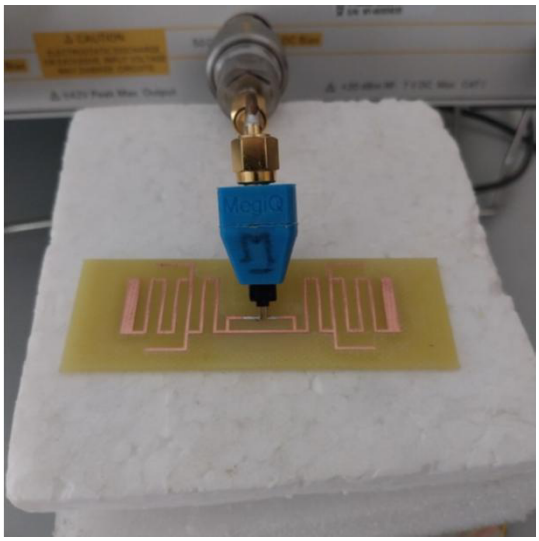

FIGURE 14. Measuring tag impedance with the Vector Network Analyzer (VNA).

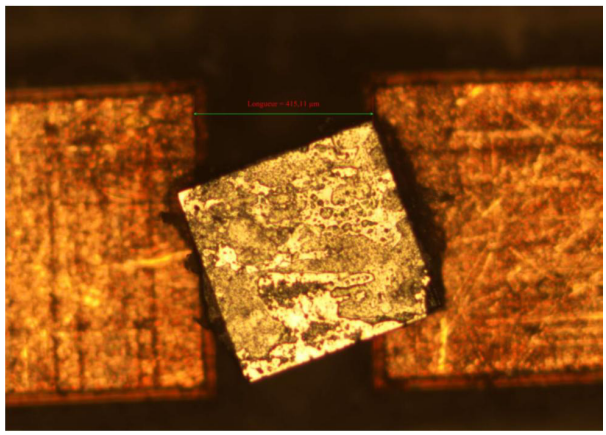

FIGURE 16. Microscopic view of the chip connected to the antenna matching circuit.

In order to validate the results obtained in simulations, it is crucial to build the prototype and then carry out measurement tests on the RFID tag.

4. REALIZED PROTOTYPE AND MEASUREMENT RESULTS

The prototype was fabricated by depositing copper onto an FR4 epoxy substrate using an electronic printer. Subsequent measurement tests were conducted to validate the simulation results. Impedance measurements were performed using a vector network analyzer (Figure 14). The impedance measurements were performed using an Agilent Technologies E5061B network analyzer, capable of operating over a broad frequency range from 5 Hz to 3 GHz. A balun from the MegiQ calibration kit was employed to facilitate the measurement of circuit parameters. This balun features two pads attached to both ends of the chip location and connects to a single port on the vector network analyzer. The two ends of the antenna gap were connected to transmission lines, which in turn were linked to the same VNA port. For the measurements, the tag was placed on foam, selected for its dielectric properties closely resembling free space.

Figure 15 presents the tag impedance measurement results over the 0.8 GHz to 1 GHz frequency range. The measurements reveal a shift in the antenna's resonant frequency, with the best impedance matching occurring at 820 MHz, where the measured impedance is $Z_a = 17.26 + \mathrm{j}109.8\,\Omega$. Although this represents the optimal match across the band, it does not perfectly correspond to the conjugate impedance of the chip. At 868 MHz, the tag exhibits reduced inductance, causing the resonant frequency to shift lower than intended.

The resonance shift can be attributed to a modification in the design parameters observed in the Gerber file. As shown in Figure 16, the gap allocated for the chip has expanded from 100 µm to 415.11 µm. This microscopic inspection reveals an approximate widening of the gap by 315 µm. Consequently, the chip was tilted to allow its tabs to connect with the radiating circuit. However, this alteration reduces the capacitive effect between the two parallel faces defining the gap, leading to an increase in the tag's reactance. As a result, the resonance frequency shifts to lower values. The observed frequency shift

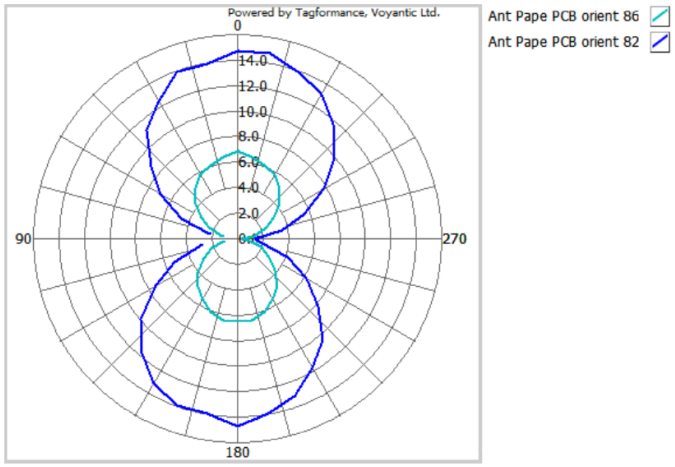

FIGURE 17. Reading distances measured at 820 MHz and 868 MHz.

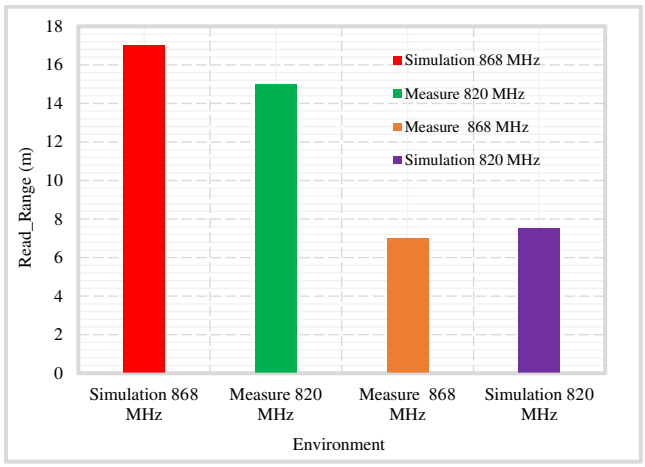

FIGURE 18. Comparison of simulated and measured read distances at 820 MHz and 868 MHz.

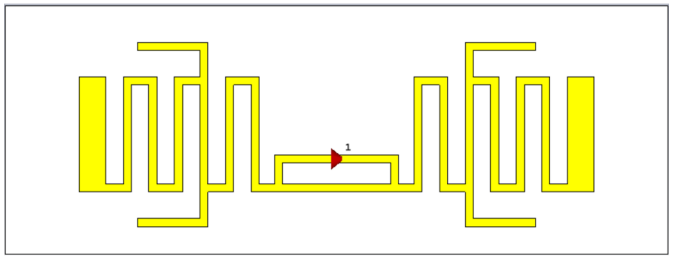

FIGURE 19. Design with Computer Simulation Technology (CST).

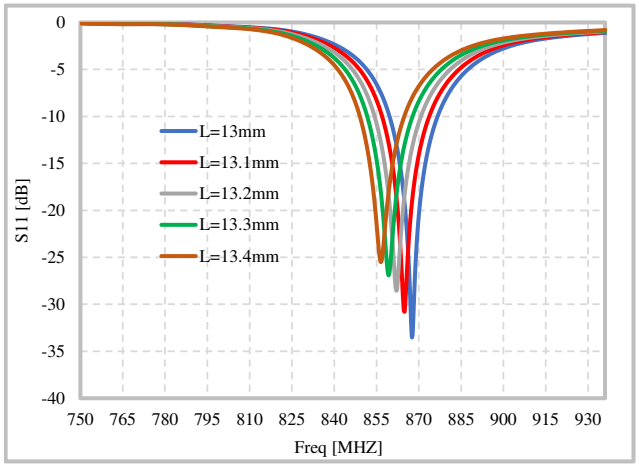

FIGURE 20. Parametric study of line length L.

from 868 MHz to 820 MHz, a difference of 48 MHz, is due to a manufacturing defect. A small variation in the dimensions of the meander lines can cause a significant shift in the resonance frequency. We will re-examine the design to find a solution to this problem.

The chip positioning proved to be challenging, which explains its tilted placement. Nevertheless, the chip's legs remain properly connected to the matching circuit lines, allowing the tag to successfully communicate with the reader.

To evaluate the label's performance, measurements of the maximum read range in free space were taken using a Voyantic Tagformance Pro system inside a mini anechoic chamber. Measurements of the tag's read distance on the vertical plane were taken at frequencies of 820 MHz and 868 MHz (Figure 17). The maximum read range, reaching up to 15 m, was obtained at 820 MHz, the frequency at which the antenna resonates. At the intended frequency of 868 MHz, the read range was approximately 7 m in free space.

Figure 18 compares the measured and simulated read ranges at 868 MHz and 820 MHz. When comparing the maximum read distances at 868 MHz, a significant discrepancy is observed. The antenna resonates at 868 MHz in simulations, while the resonance frequency obtained during measurements is 820 MHz. the simulated range is approximately 17 m, while the measured maximum is only 7 m, resulting in a 10 m difference. At the target frequency of 868 MHz, the reading range in free space is approximately 7 m. Since the tag's performance is limited within this frequency band, a meaningful comparison with the simulation results is not feasible. Therefore, it is necessary to re-examine the design to identify the root cause of this discrepancy and develop a new prototype that effectively covers the European UHF RFID band (865.5–869.5 MHz).

Measurements on the various surfaces intended for labeling with this prototype were not conducted, as the impedance matching issue needed to be resolved before proceeding.

To address this, the design was re-simulated using CST Studio microwave simulation software. In this iteration, the substrate was changed to Taconic RF-35A2 ($\varepsilon_r = 3.5$; $\tan\sigma = 0.0018$), and the tag parameters were readjusted accordingly. Figure 19 presents a top view of the redesigned tag in CST, preserving the original structural configuration.

The modified parameters include the substrate width Ws set to 28 mm and the length L of the meander lines. Initially, the tag was simulated with all original parameters except for the substrate width, which was increased from 25 mm to 28 mm. The simulation showed that the antenna resonates at 856 MHz, resulting in a 12 MHz offset from the target frequency of 868 MHz.

Subsequently, a parametric study was performed by varying the meander line length L from 13 mm to 13.4 mm in 0.1 mm increments. This analysis identified that a meander line length of 13 mm yields resonance at the desired 868 MHz frequency (Figure 20).

The prototype was then fabricated, and measurements of impedance and reading range were conducted to validate the simulation results. The fabrication involved engraving a 35 µm thick copper layer onto a Taconic RF-35A substrate. Impedance matching measurements were performed using a vector network analyzer (VNA) prior to chip placement, as illustrated in Figure 21.

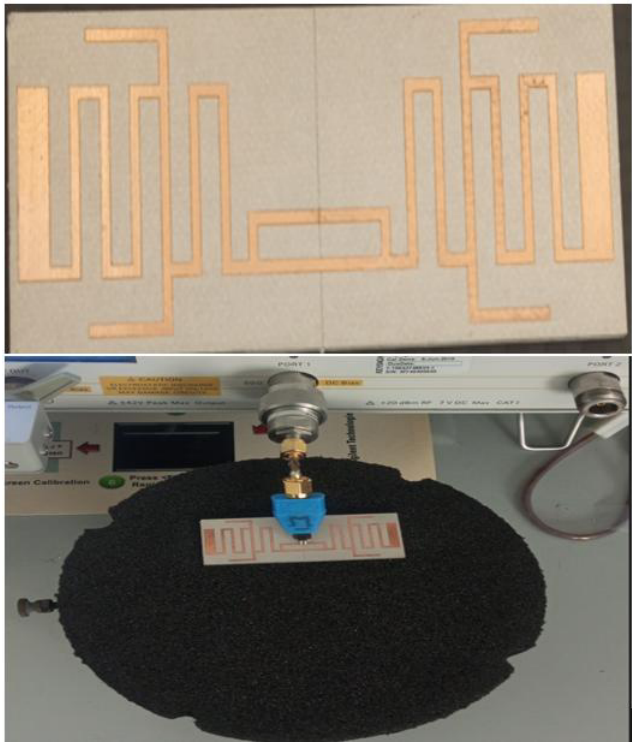

FIGURE 21. The prototype and measurement with the VNA.

Figure 22 shows the simulated and measured reflection coefficients of the tag in free space. A slight frequency shift is observed in the measured resonance compared to the simulation results. The measured reflection coefficient indicates a resonance at 878 MHz with an S_{11} value of -14 dB, representing a 10 MHz offset from the simulated resonance.

Since the manufactured prototype did not match the dimensions of the original design, a new simulation was performed using the prototype's actual dimension, $L_s = 60$ mm. As shown in Figure 22, this updated simulation aligns well with the measurement results, demonstrating that both the simulated and measured tags cover the same frequency band.

The simulated impedance at 868 MHz is $Z_a = 13.6 + \mathrm{j}125\,\Omega$ losely matching the conjugate impedance of the Monza R6 chip, $Z_c^* = 13 + \mathrm{j}125\,\Omega$ Vector network analyzer (VNA) measurements confirm a good match, with the measured resistance near 12 Ω and a slight offset in the reactance at approximately 113

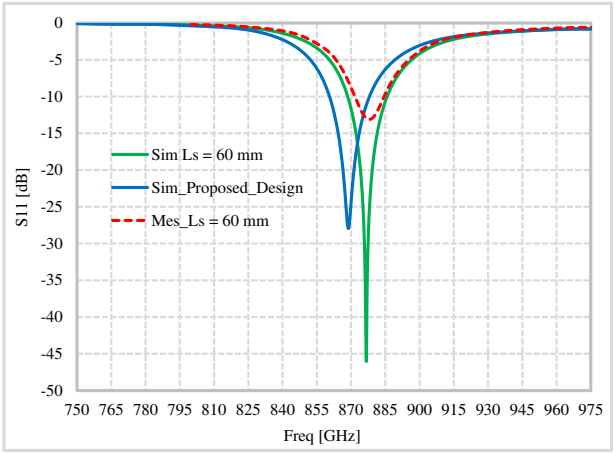

FIGURE 22. The simulated and measured reflection coefficients of the tag in free space.

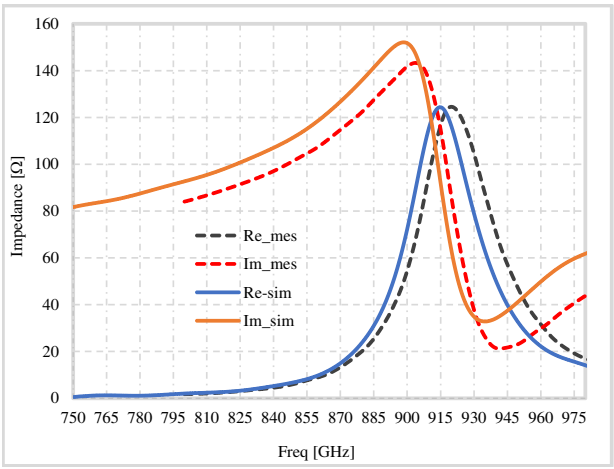

FIGURE 23. Simulated and measured impedances of the tag in free space.

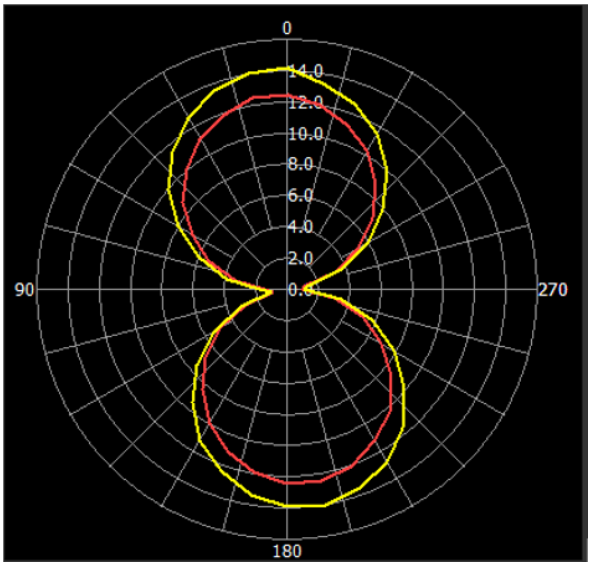

FIGURE 24. Reading distance measured in free space at 868 MHz and 878 MHz.

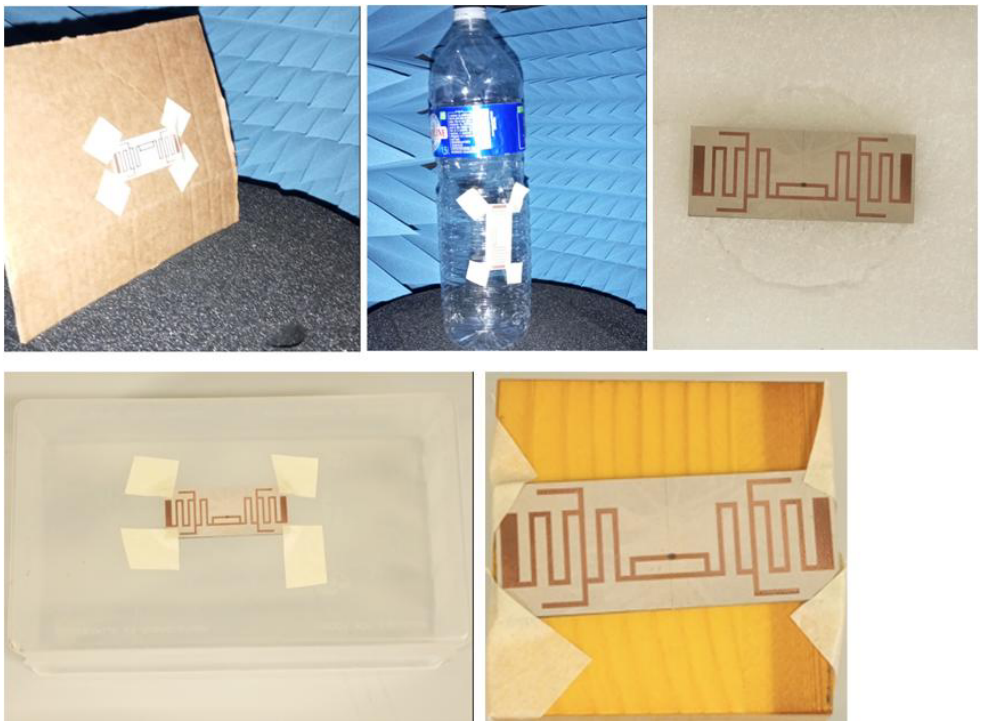

FIGURE 25. Surfaces tagged for measurement tests.

at 868 MHz, as shown in Figure 23. These discrepancies are explained by the dimensional variations discussed above.

After placing the Monza R6 chip, tag performance tests are carried out by measuring the tag's maximum read range.

To validate the tag's radiation performance, measurements of its reading distance were first conducted in free space, as the antenna was originally designed and simulated under these conditions (Figure 24). Subsequent measurements on the various specified surfaces will follow.

To assess the tag's performance on complex surfaces, it was placed on foam, an empty PET bottle, cardboard, a plastic box, and wood. These measurements evaluated the tag's robustness against variations in the surfaces to be identified.

Figure 25 illustrates the different surfaces tagged with the proposed design. These materials are typical in transportation sector for product routing and were chosen to test the tag's performance in realistic applications.

Measurements of the tag's reading range were conducted to determine its radiation performance across the 800 MHz to 1000 MHz band on these surfaces (Figure 26). The results show that the maximum read distance in free space reaches approximately 13.8 meters at 868 MHz within the European UHF RFID band. The resonance frequency remains stable on free space, foam, and the empty PET bottle, with the maximum reading distance achieved around 868 MHz.

Interestingly, the highest maximum reading distance of 14.2 meters is obtained when the tag is mounted on the PET bottle, compared to 12.4 meters on foam. When placed on cardboard and the plastic box, the tag's resonance shifts to approximately 860 MHz, reflecting an increased frequency shift. The measured reading distances at 868 MHz in the European UHF RFID

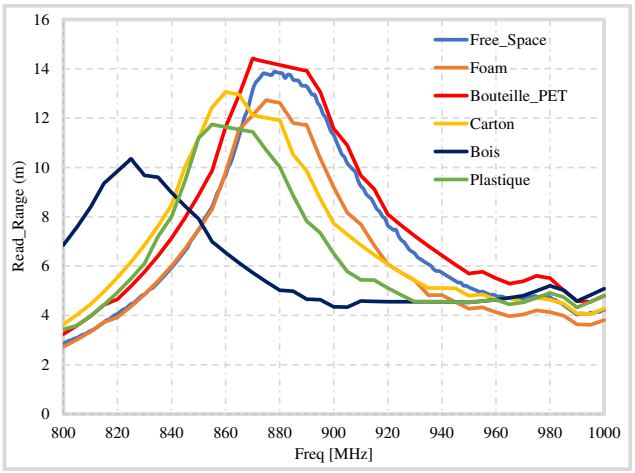

FIGURE 26. Measured tag reading distance in different environments.

band are 12.0 meters on cardboard and 11.5 meters on the plastic box.

Mounting the tag on wood causes a notable resonance shift towards lower frequencies, with the maximum reading distance at these frequencies reduced to around 6 meters in the European UHF RFID band.

The variation in the measured reading distance across different objects confirms the theoretical reading range predicted by the Friis equation (Figure 13).

The tag is effective in identifying various complex surfaces and encounters no reading issues on any of them. Although the resonant frequency shifts depending on the surface, the reading

TABLE 4. Comparative study with some previous works.

Ref	Size (mm^2)	Surface tagged	Freq	Distance
[1]	65×15	Plastic Bottle Glass Bottle Water Liquids	915 MHz	6.5 m 2.6 m > 2 m
[12]	40×20	Plastic Bottle Water Bottle	915 MHz	8 m 4.2 m
[15]	40×20	Plastic Box Fiber Wood Glass	915 MHz	3.5 m 10 m 6 m 1.5 m
[16]	40×20	Foam Fiber Wood Glass	866 MHz and 912 MHz	5 m 5 m 4.5 m 3.5 m
Work	75×28	Plastic Bottle Plastic box Wood Cardboard	868 MHz	14.2 m 11.5 m 6 m 12 m

distance remains substantial in all cases, with the shortest range being 6 meters at 868 MHz. These results demonstrate that the proposed tag is well suited for product tracking applications in supply chain environments involving diverse and complex surfaces.

Figure 27 compares the measured read ranges in different environments with simulation results at the key frequency of 868 MHz. On all tested surfaces, including free space, foam, PET bottles, cardboard, and wood, the measured reading distances are close to those simulated. This agreement demonstrates the robust performance of the proposed tag on various complex tagged surfaces.

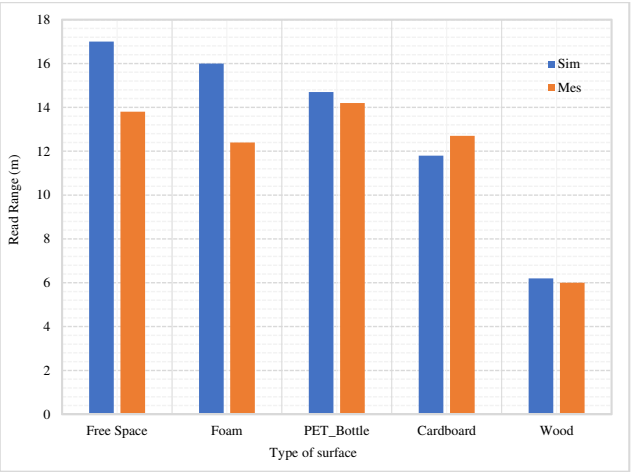

FIGURE 27. Comparison of simulated and measured reading distances at 868 MHz on various complex surfaces.

Table 4 provides a comparative study between the performance of the proposed tag design and other prior works. This highlights the competitive advantages of the current design in terms of read range and adaptability to complex surfaces commonly used in supply chain and product tracking applications.

To evaluate the performance of the proposed UHF RFID tag for identifying complex surfaces commonly used in transportation sector, a comparison with previously reported prototypes was made based on the type of surface tagged and the maximum reading distance achieved.

The prototypes described in [1] and [12] demonstrate good performance on certain complex surfaces such as plastic bottles, wood, and cardboard. Those reported in [15] and [16] target objects including foam, fiber, plastic boxes, wood, and glass materials more closely related to those considered in our study. Our paper makes a significant contribution by demonstrating superior read range performance and exceptional adaptability across multiple complex surfaces compared to previous designs. As detailed in Table 4, our prototype achieves a maximum reading range of 14.2 meters on plastic bottles, and importantly, maintains a minimum range of 6 meters even on challenging wood surfaces, all at 868 MHz. This significantly surpasses the read ranges reported in similar works (e.g., [1, 12, 15, 16]), which often show more limited ranges or are less adaptable across such a broad spectrum of materials.

5. CONCLUSION

This paper has presented a passive UHF RFID dipole tag designed for product identification in the supply chain. The initial design, simulated using HFSS, exhibited discrepancies between simulation and measurement results due to a design flaw. A redesigned tag, employing a different substrate and adjusted antenna parameters, delivered measurement results that closely matched simulations. Reading distance measurements on various complex surfaces, including foam, plastic bottles, wood, and cardboard, demonstrated that the maximum read range was approximately 14.2 meters on a plastic bottle and the minimum was around 6 meters on wood, both measured at 868 MHz.

REFERENCES

[1] Sharif, A., R. Kumar, J. Ouyang, H. T. Abbas, A. Alomainy, K. Arshad, K. Assaleh, A. Althuwayb, M. A. Imran, and Q. H. Abbasi, "Making assembly line in supply chain robust and secure using UHF RFID," *Scientific Reports*, Vol. 11, No. 1, 18041, 2021.

[2] Sarr, P. W., I. Dioum, and A. Diop, "Robust RFID antenna for tracking health products and water bottles," in *2023 IEEE 13th International Conference on RFID Technology and Applications (RFID-TA)*, 119–122, Aveiro, Portugal, 2023.

[3] Bouhassoune, I., H. Chaibi, A. Chehri, and R. Saadane, "UHF RFID spiral-loaded dipole tag antenna conception for healthcare applications," *Procedia Computer Science*, Vol. 192, 2531–2539, 2021.

[4] Diallo, A., P. L. Thuc, S. Lanteri, and G. F. Carle, "Antenne miniature implantée pour applications RFID UHF," in *20èmes Journées Nationales Microondes (JNM 2017)*, 4, Saint-Malo, France, 2017.

[5] Sharif, A., Y. Yan, J. Ouyang, H. T. Chattha, K. Arshad, K. Assaleh, A. A. Alotabi, T. Althobaiti, N. Ramzan, Q. H. Abbasi, and M. A. Imran, "Uniform magnetic field characteristics based UHF RFID tag for internet of things applications," *Electronics*, Vol. 10, No. 13, 1603, 2021.

[6] Hussain, M., Y. Amin, and K.-G. Lee, "A compact and flexible UHF RFID tag antenna for massive IoT devices in 5G system," *Sensors*, Vol. 20, No. 19, 5713, 2020.

[7] Byondi, F. K. and Y. Chung, "Longest-range UHF RFID sensor tag antenna for IoT applied for metal and non-metal objects," *Sensors*, Vol. 19, No. 24, 5460, 2019.

[8] Rao, K. V. S., "An overview of backscattered radio frequency identification system (RFID)," in *1999 Asia Pacific Microwave Conference. APMC'99. Microwaves Enter the 21st Century. Conference Proceedings (Cat. No.99TH8473)*, Vol. 3, 746–749, Singapore, 1999.

[9] Köny, M., M. Walter, T. Schlebusch, and S. Leonhardt, "An RFID communication system for medical applications," in *2010 International Conference on Body Sensor Networks*, 71–75, Singapore, 2010.

[10] Chawla, V. and D. S. Ha, "An overview of passive RFID," *IEEE Communications Magazine*, Vol. 45, No. 9, 11–17, 2007.

[11] Riaz, M., G. Rymar, M. Ghavami, and S. Dudley, "A novel design of UHF RFID passive tag antenna targeting smart cards limited area," in *2018 IEEE International Conference on Consumer Electronics (ICCE)*, 1–4, Las Vegas, NV, USA, 2018.

[12] He, S., Y. Zhang, L. Li, Y. Lu, Y. Zhang, and H. Liu, "High performance UHF RFID tag antennas on liquid-filled bottles," *Progress In Electromagnetics Research*, Vol. 165, 83–92, 2019.

[13] Claucherty, E., D. Cummins, A. Rossi, and B. Aliakbarian, "Effect of beverage composition on radio frequency identification (RFID) performance using polyethylene terephthalate (PET) bottles for smart food packaging applications," *Foods*, Vol. 13, No. 5, 643, 2024.

[14] Bansal, A., S. Sharma, and R. Khanna, "Platform tolerant dual-band UHF-RFID tag antenna with enhanced read range using artificial magnetic conductor structures," *International Journal of RF and Microwave Computer-Aided Engineering*, Vol. 30, No. 2, e22065, 2020.

[15] Bansal, A., S. Sharma, and R. Khanna, "Compact meandered RFID tag antenna with high read range for UHF band applications," *International Journal of RF and Microwave Computer-Aided Engineering*, Vol. 29, No. 11, e21695, 2019.

[16] Bansal, A., S. Sharma, and R. Khanna, "Compact meandered folded-dipole RFID tag antenna for dual band operation in UHF range," *Wireless Personal Communications*, Vol. 114, No. 4, 3321–3336, 2020.

[17] Sarr, P. W., I. Dioum, A. Diop, D. Ba, M. M. Khouma, and I. Gueye, "A new broadband compact meander dipole antenna for RFID applications," in *2022 International Conference on Electrical, Computer and Energy Technologies (ICECET)*, 1–6, Prague, Czech Republic, 2022.

[18] Unhelkar, B., S. Joshi, M. Sharma, S. Prakash, A. K. Mani, and M. Prasad, "Enhancing supply chain performance using RFID technology and decision support systems in the industry 4.0 — A systematic literature review," *International Journal of Information Management Data Insights*, Vol. 2, No. 2, 100084, 2022.

[19] Varriale, V., A. Cammarano, F. Michelino, and M. Caputo, "Integrating blockchain, RFID and IoT within a cheese supply chain: A cost analysis," *Journal of Industrial Information Integration*, Vol. 34, 100486, 2023.

[20] Nayak, R., M. George, I. U. Haq, and H. C. Pham, "Sustainability benefits of RFID technology in Vietnamese fashion supply chain," *Cleaner Logistics and Supply Chain*, Vol. 5, 100086, 2022.

[21] Xue, F., Y. Zhang, J. Li, and H. Liu, "Circularly polarized cross-dipole antenna for UHF RFID readers applicated in the warehouse environment," *IEEE Access*, Vol. 11, 38 657–38 664, 2023.

[22] Kusuda, K., K. Yamashita, E. Morishita, N. Ishibashi, Y. Shiraishi, and H. Yamaguchi, "Comparison of reading times of RFID-tagged and barcode-engraved surgical instruments," *Journal of Surgical Research*, Vol. 304, 121–125, 2024.

[23] Zannas, K., F. P. Chietera, A. Abdelnour, D. Kaddour, R. Colella, L. Catarinucci, Y. Duroc, and S. Tedjini, "Designing UHF RFID tag antennas with barcode shape for dual-technology identification," *IET Microwaves, Antennas & Propagation*, Vol. 16, No. 12, 733–742, 2022.

[24] Kubáňová, J., I. Kubasáková, K. Čulík, and L. Štítik, "Implementation of barcode technology to logistics processes of a company," *Sustainability*, Vol. 14, No. 2, 790, 2022.

[25] Suresh, S. and G. Chakaravarthi, "RFID technology and its diverse applications: A brief exposition with a proposed Machine Learning approach," *Measurement*, Vol. 195, 111197, 2022.

[26] Casula, G. A., G. Montisci, and G. Mazzarella, "A wideband PET inkjet-printed antenna for UHF RFID," *IEEE Antennas and Wireless Propagation Letters*, Vol. 12, 1400–1403, 2013.

[27] Griffin, J. D., G. D. Durgin, A. Haldi, and B. Kippelen, "Radio link budgets for 915 MHz RFID antennas placed on various objects," in *Texas Wireless Symposium*, Vol. 44, 2005.

[28] Bong, F.-L., K. Thirappa, E.-H. Lim, and K. Perumal, "Compact metal-mountable UHF RFID tag antenna with two large C-shaped slots for on-the-fly tuning," *Progress In Electromagnetics Research M*, Vol. 101, 173–183, 2021.

[29] Saghlatoon, H., L. Sydänheimo, L. Ukkonen, and M. Tentzeris, "Optimization of inkjet printing of patch antennas on low-cost fibrous substrates," *IEEE Antennas and Wireless Propagation Letters*, Vol. 13, 915–918, 2014.

[30] Zuffanelli, S., P. Aguila, G. Zamora, F. Paredes, F. Martin, and J. Bonache, "A high-gain passive UHF-RFID tag with increased read range," *Sensors*, Vol. 16, No. 7, 1150, 2016.

[31] Marrocco, G., E. D. Giampaolo, and R. Aliberti, "Estimation of UHF RFID reading regions in real environments," *IEEE Antennas and Propagation Magazine*, Vol. 51, No. 6, 44–57, 2009.